



Contents lists available at ScienceDirect

Micron

journal homepage: [www.elsevier.com/locate/micron](http://www.elsevier.com/locate/micron)

## *In situ* TEM studies of oxygen vacancy migration for electrically induced resistance change effect in cerium oxides

Peng Gao, Zhenzhong Wang, Wangyang Fu, Zhaoliang Liao, Kaihui Liu, Wenlong Wang, Xuedong Bai<sup>\*</sup>, Enge Wang<sup>\*\*</sup>

Beijing National Laboratory for Condensed Matter Physics, Institute of Physics, Chinese Academy of Sciences, Beijing 100190, China

### ARTICLE INFO

#### Article history:

Received 15 October 2009  
Received in revised form 30 November 2009  
Accepted 30 November 2009

#### Keywords:

*In situ* TEM  
Microscopic mechanism  
Oxygen vacancy migration  
Resistance change effect  
CeO<sub>2</sub>

### ABSTRACT

Oxide materials with resistance hysteresis are very promising for next generation memory devices. However, the microscopic dynamic process of the resistance change is still elusive. Here, we use *in situ* transmission electron microscopy method to study the role of oxygen vacancies for the resistance switching effect in cerium oxides. The structure change during oxygen vacancy migration in CeO<sub>2</sub> induced by electric field was *in situ* imaged inside high-resolution transmission electron microscope, which gives a direct evidence for oxygen migration mechanism for the microscopic origin of resistance change effect in CeO<sub>2</sub>. Our results have implications for understanding the nature of resistance change in metal oxides with mixed valence cations, such as fluorite, rutile and perovskite oxides.

© 2009 Elsevier Ltd. All rights reserved.

### 1. Introduction

Recently, a large number of insulating oxides with resistance switching effect have attracted extensive interest, ranging from simple binary oxides of rutile, fluorite and related structures (e.g., TiO<sub>2</sub> (Yang et al., 2008), CeO<sub>2</sub> (Fors et al., 2005)), to the complex three-, four- and five-component perovskites and related structures (e.g., SrTiO<sub>3</sub> (Szot et al., 2006), Cr-doped SrTiO<sub>3</sub> (Beck et al., 2000) and Pr<sub>1-x</sub>Ca<sub>x</sub>MnO<sub>3</sub> (Liu et al., 2000)). Devices based on these oxides are very promising for next generation memories due to their non-volatile, high density, fast and small power-consuming properties. For the realization of practical application, it is important to understand and control the coupled electronic and ionic phenomena that dominate the switching behavior of nanoscale oxide devices.

Several models have been proposed to explain the resistance switching effect, including Mott transition (Fors et al., 2005; Oka and Nagaosa, 2005), Schottky barrier behavior at the interface (Sawa et al., 2004; Fujii et al., 2005), charge trapping or detrapping (Rozenberg et al., 2004), polaron melting and ordering (Jooss et al.,

2007), electric field-induced generation of crystalline defects (Tsui et al., 2006; Hamaguchi et al., 2006), creation or destruction of 'conducting filament' (Szot et al., 2006) and oxygen vacancy diffusion (Baikalov et al., 2003; Nian et al., 2007; Janousch et al., 2007; Quintero et al., 2007). Because oxygen vacancies widely exist in metal oxides, oxygen migration model could be one of the important understandings for the origin of the resistance switching effect, although the direct experimental evidences are still needed. According to this model, the oxygen vacancies (ions) are the active agents for resistance switching effect. The mobility of oxygen vacancies is enhanced and thereby their pileup near metal electrodes is caused under the applied electric field during a switching operation. Thus, a local change of concentration of oxygen vacancies near the electrodes results in changing the resistance. The low resistance state (LRS) can be imagined as a conductive path between the two electrodes that turn on the devices. The high resistance state (HRS) may be described as the destruction of this conductive path as the devices are turned off. However, the observation of microscopic dynamic process of the oxygen vacancy migration at atomic level is absent. One solution for probing and analyzing the oxygen diffusion for resistance switching effect is to measure the local transport property and monitor the structural evolutions simultaneously by *in situ* transmission electron microscopy (TEM) method. Such an approach is significant but rarely reported (Jooss et al., 2007). For many oxides with mixed valence cations (for example, transition-metal oxides and rare-earth metal oxides), the oxygen vacancies are mobile, while the cations sublattices are stable. It is believed

<sup>\*</sup> Corresponding author at: Beijing National Laboratory for Condensed Matter Physics, Institute of Physics, Chinese Academy of Sciences, 83rd South ST of Zhongguancun, Beijing 100190, China. Tel.: +86 10 8264 8032; fax: +86 10 8264 9228.

<sup>\*\*</sup> Corresponding author.

E-mail addresses: [xdbai@aphy.iphy.ac.cn](mailto:xdbai@aphy.iphy.ac.cn) (s.S. Bai), [egwang@aphy.iphy.ac.cn](mailto:egwang@aphy.iphy.ac.cn) (E. Wang).

that the generation and the destruction of the conducting path are associated with the oxygen migration.

Here, we report on a direct evidence for oxygen migration mechanism for electrically induced resistance change effect in Au/CeO<sub>2</sub>/Nb-STO (Nb doped SrTiO<sub>3</sub>) heterostructures by using *in situ* TEM method. We have directly observed the dynamic process of resistance switching operation accompanying with oxygen migration in the cerium oxides at atomic level. Based on these observations, it is found that the formation of path of neighboring oxygen vacancies could be the origin of the resistance switching effect in cerium oxides. Our results may also be extended to other oxide systems that have mixed valence cations.

## 2. Experiments

Experimentally, epitaxial CeO<sub>2</sub> films are grown by pulsed-laser deposition (PLD) on Nb-STO (1 0 0) substrates (0.7% Nb doped SrTiO<sub>3</sub>), with different thicknesses ranging from 20 to 200 nm. The growth direction of CeO<sub>2</sub> film is [1 0 0] (data not shown here). We first fabricated Au electrodes on top of the CeO<sub>2</sub> film to form the sandwiched structures using a standard photolithographic technique and magnetron sputtering. Typical *I*–*V* characteristics of Au/CeO<sub>2</sub>/Nb-STO device are shown in Fig. 1. The loops, 0 → +*V*<sub>max</sub> → 0 → –*V*<sub>max</sub> → 0, were demonstrated and they have high degree of repeatability. Positive voltages are corresponding to positive biases applied on the gold electrode, while the bottom electrode (metallic Nb-STO has good electric conductivity, as shown in inset of Fig. 1) was grounded. To show the resistance switching effect, the applied voltages were swept from a HRS (curve 1) until the decrease of the resistance after a positive bias threshold (~1.5 V). This means the conducting path was generated between the electrodes. The device would stay at the LRS even bias decrease (curve 2 and curve 3) until the negative threshold voltage (~–4 V) is overcome, whereby the conducting path was broken down and the resistance increases notably, then the device went back to the HRS (curve 4). If the sweeping voltage is less than the threshold voltage, there is no creation or destruction of the conducting path. The reversible *I*–*V* characteristics have been shown for the following sweeping cycles. Now, the remaining question is the structural and chemical properties of the conducting path.

To explore the microscopic dynamic process for the resistance switching effect, we first made sample Au/CeO<sub>2</sub>/Nb-STO junction for *in situ* TEM measurements. The electron transparent cross-section samples were prepared by conventional mechanical polishing and argon ion milling to a thickness of around 30–60 nm. Then a bias voltage was applied across the sandwiched

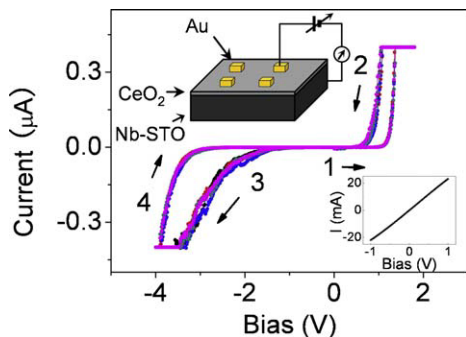


**Fig. 1.** *I*–*V* characteristics of single crystalline (1 0 0) CeO<sub>2</sub> device with Nb-STO (0.7% Nb doped SrTiO<sub>3</sub>) bottom electrode and Au top electrode. The upper inset: schematic drawing of the junction with electrode geometry in which Au is taken to be positive. The thickness of CeO<sub>2</sub> film is about 40 nm. The dimension of the Au electrode is 100 μm × 100 μm, 30 nm thick and with a 600 μm separation in two directions. The lower inset: the measurement of the resistance of Nb-STO substrate, which shows good electric conductivity (~50 Ω).

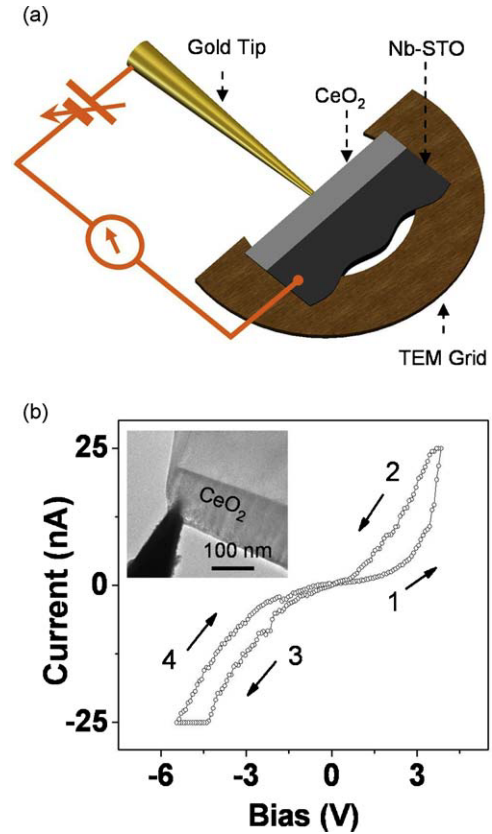


**Fig. 2.** (a) Scheme of *in situ* TEM measurement setup. The cross-section TEM-ready sample, CeO<sub>2</sub>/Nb-STO junction, was contacted by a gold tip at a selected position by piezo-controller, measuring the resistance and monitoring the structural evolution simultaneously. (b) A loop of *in situ* *I*–*V* sweep reveals the resistance switching effect. The inset: TEM image of metal-tip/CeO<sub>2</sub>/Nb-STO structure.

junction inside a TEM (JOEL 2010F microscope with vacuum  $2 \times 10^{-5}$  Pa at room temperature) as illustrated in Fig. 2a. A sharp gold tip driven by piezo-controller moved forward to contact the CeO<sub>2</sub> film of TEM-ready cross-section sample which loaded on a home-made specimen holder. For electrical measurements, the TEM electron beam was blanked out. The loop of *in situ* *I*–*V* sweep also displayed the resistance switching effect, as shown in Fig. 2b.

## 3. Results and discussion

### 3.1. Structure

Fig. 3a and b show the high-resolution TEM image and the electron diffraction pattern detected along the  $\langle 110 \rangle$  axis before applying electric field, and Fig. 3c displays the solid sphere model. By applying a bias of 1 V to the junction for a few seconds [the device is still at the HRS], both the TEM image and the diffraction pattern remained unchanged. Then we applied a bias of 5 V to make sure the device was at LRS (electric field  $E \sim 7.5 \times 10^7$  V/m), as shown in Fig. 3d, the structural transition took place with the appearance of wavy structures in the high-resolution TEM image. The extra diffraction spots were also observed (Fig. 3e). These superlattice reflections indicate that oxygen anions had been removed from the ceria film and the introduced oxygen vacancies were ordered as Ce<sub>2</sub>O<sub>3</sub> by the applied electric field (Wang and Kang, 1998; Sharma et al., 2004; Crozier et al., 2008). The structure model for the process of forming ordered oxygen vacancies is represented in Fig. 3f, where the rectangle shows the unit cell of sesqui-oxide of the cerium oxide in the  $\langle 110 \rangle$  orientation resulted by ordered oxygen vacancies.

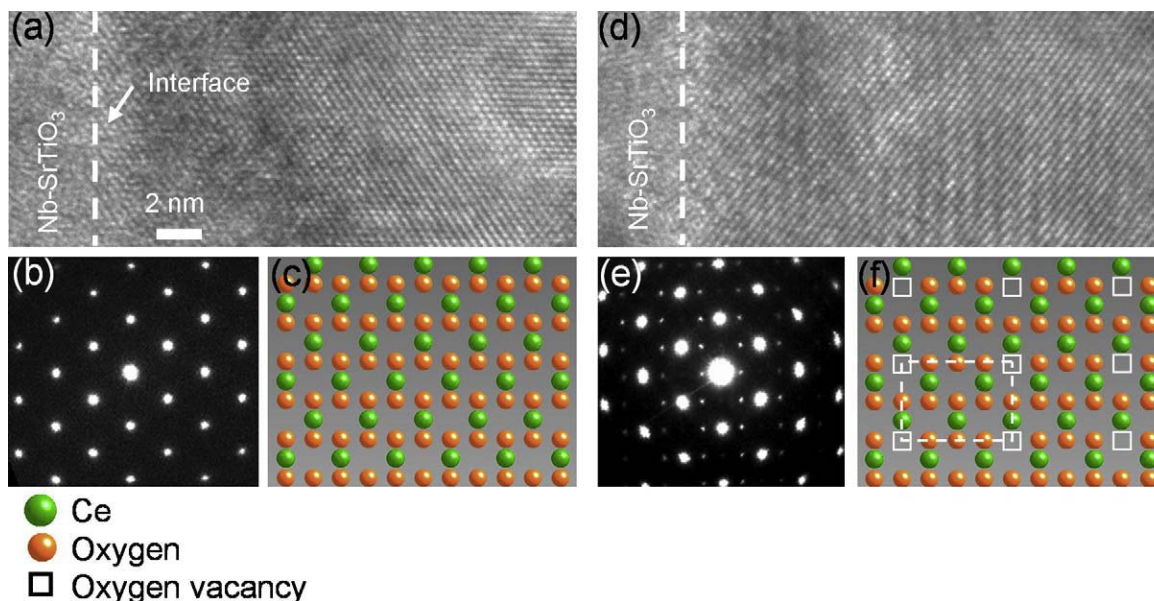


**Fig. 3.** (a) Atomic TEM image of ceria single crystal film along (110) zone axes. (b) Corresponding electron diffraction pattern. (c) Solid sphere model of  $\text{CeO}_2$  in a perfect fluorite structure. (d) When 5 V voltage ( $E \sim 7.5 \times 10^7 \text{ V/m}$ ) was applied between the gold tip and Nb-STO, the superlattice reflections appeared. The gold tip was positive electrode. (e) Extra diffraction spots appeared. (f) Solid sphere model showing the formation of oxygen vacancies. The rectangles indicate the vacancy superlattices.

### 3.2. EELS

Because oxygen vacancy migration is accompanied with the valence change in oxides, to gain further evidence of the oxygen vacancy diffusion process, we have performed electron energy loss spectroscopy (EELS) experiments on the samples to show the change of chemical valence of the Ce ions. When applying a bias of 5 V, a reversal in the intensity of Ce  $M_{45}$ -white lines was observed [Fig. 4a and b], suggesting that Ce has undergone a transition from  $4+$  to  $3+$  oxide state (Garvie and Buseck, 1999). The disappearance of the shoulder (indicated by arrowhead in Fig. 4a) suggests that the strong covalence hybridization between Ce  $4f$  and O  $2p$  states was vanished under the applied electric field. In fact, the influence of TEM electron beam irradiation can be ruled out in this study. We found that significant change in the white-line ratio occur by dose more than  $1.8 \times 10^6 \text{ electron}/\text{\AA}^2$  from a sample with about 35 nm thickness at the edge region, and in our *in situ* TEM experiments, we kept the electron dose lower than  $3 \times 10^5 \text{ electron}/\text{\AA}^2$ , which should ensure that our measured changes in Ce oxidation state under the electric field are not caused by electron irradiation.

### 3.3. Mechanism

The cerium oxide is facile to create anion deficiency because the oxygen anions of fluorite structure are very active, and can move through the lattice relatively easily (Trovarelli, 1996). In the presence of electric field (positive bias on the Au electrode), the oxygen anions ( $\text{O}^{2-}$ ) will move toward the anode where they have taken electron and evolve oxygen gas. Concurrently, the oxygen vacancies will diffuse into the crystal interior, and then assembled near the cathode to reduce  $\text{CeO}_2$  to  $\text{Ce}_2\text{O}_3$ . For stoichiometric  $\text{CeO}_2$ , which is an insulator with band gap 6 eV (Koelling et al., 1983), the oxygen p band has two extra electrons provided by Ce atom and there is a narrow empty Ce f band in the gap between the valence and conducting bands, as shown in Fig. 5. When an oxygen atom is leaving its lattice position, the two electrons may occupy the lowest possible empty state that is the f band of nearest Ce atoms, tuning  $\text{Ce}^{4+}$  to  $\text{Ce}^{3+}$  with electron hopping (Skorodumova et al., 2002). It means that the oxygen migration process simultaneously accompanies with the ionic and electron conductivity. The presence of  $\text{Ce}^{3+}$  ions (or oxygen vacancies) enhances the local

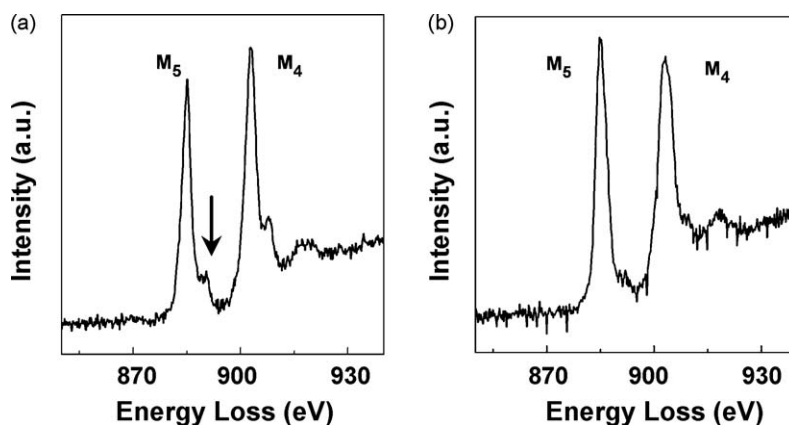


**Fig. 4.** (a) EEL spectra of Ce-M edge at zero bias. (b) A reversal in the intensity of Ce  $M_{45}$  white lines was observed; and the shoulder indicated by arrow in (a) disappeared after applying the electric field.

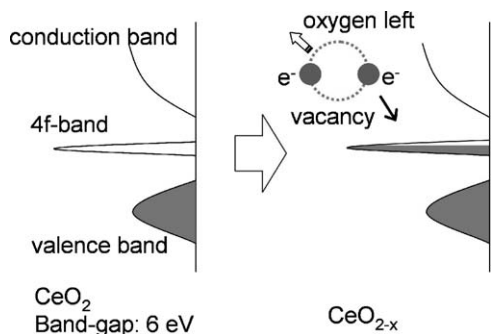


**Fig. 5.** Left: the energy band of perfect  $\text{CeO}_2$ , whose band gap is 6 eV (Koelling et al., 1983). There is a narrow empty Ce 4f band in the gap. Right: the energy band of  $\text{CeO}_{2-x}$ . When an oxygen atom moves away from their lattice positions, the two electrons will localize on cerium atoms (transition from  $\text{Ce}^{4+}$  to  $\text{Ce}^{3+}$ ). Thus, the electron conductivity is enhanced.

electron conductivity of the cerium oxide (band gap of  $\text{Ce}_2\text{O}_3$  is about 2.4 eV (Prokofiev et al., 1996)). In the electric field, if the domain of  $\text{Ce}^{3+}$  ions bridged the two electrodes, conductive paths will be formed and the device will be switched from HRS to LRS.

In the case of a sufficient negative voltage on the Au electrode, the oxygen anions are driven to move toward the interface of  $\text{CeO}_2/\text{Nb-STO}$  (anode). As we know, the  $\text{CeO}_2$  layer is blanket film and epitaxial growth on the STO, so the oxygen anions will be blocked by interface, and cannot be released as easily as at the surface (at the metal electrode). The cerium oxide film near the interface would likely form the stoichiometric dioxide ( $\text{CeO}_2$ ) and turn off the conducting path, and hence the high resistance state (HRS). At the same time, the vacancies migrate to the surface (at metal electrode). Oxygen gas will infuse into the metal/ $\text{CeO}_2$  interface layer due to that the density of the vacancies near the surface region is higher than the equilibrium concentration. Fig. 6 shows the vacancies could be recovered and the wave sweeping disappeared when  $-7\text{ V}$  bias applied to the gold tip. It is worthy to point out that the residual oxygen in the chamber of the TEM is enough to recover the vacancies even under the vacuum of approximately  $10^{-5}\text{ Pa}$  (Bevan and Kordis, 1964).

Moreover, the communication between oxygen anions and gas oxygen is also found in a number of other oxides (Waser and Aono, 2007). For instance, Szot et al. (2006) discovered that gas bubbles had developed under the anode when the electric field was applied to single crystalline  $\text{SrTiO}_3$ . From measuring the fatigue behavior of  $\text{Ag}/\text{La}_{0.7}\text{Ca}_{0.3}\text{MnO}_3/\text{Pt}$  heterostructures, Shang et al. (2007) proposed that oxygen gas could infuse into the electrode/film interface and oxygen anions could diffuse out to the environment when different bias was applied. Yoshida et al. (2008) demonstrated that the gas oxygen could penetrate into the non-stoichiometric nickel oxide film using  $^{18}\text{O}$  tracer gas atmosphere. More recently, Yang et al. (2009) also found bubbles had formed along the edge of the bottom electrode in  $\text{TiO}_2$  devices. For fluorite structure, oxygen is also easily migrated in cerium oxide driven by

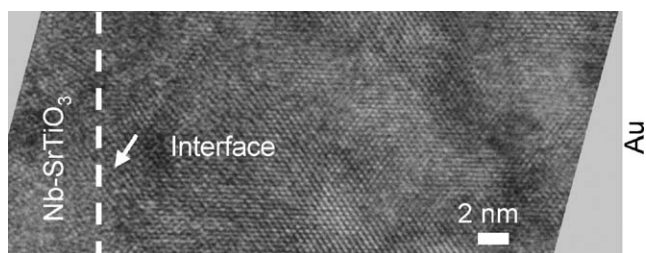


**Fig. 6.** The TEM image after a voltage of  $-7\text{ V}$  was applied between the gold tip and Nb-STO. The white line (left) indicates the interface of the  $\text{CeO}_2/\text{Nb-STO}$ .

the electric field (Bevan and Kordis, 1964; Trovarelli, 1996), which was directly imaged *in situ* TEM in this study.

#### 4. Conclusion

In summary, we have studied the role of oxygen vacancy migration for the electrically induced resistance effect in  $\text{Au}/\text{CeO}_2/\text{Nb-STO}$  junctions by using *in situ* TEM method. For the first time, the dynamic process of resistance switching accompanying with the oxygen migration has been directly imaged at atomic level. Our *in situ* TEM studies unambiguously demonstrate that the migration of the oxygen vacancies is responsible for the resistance switching effect in cerium oxides. This mechanism might provide new insight on the physical and chemical nature of resistance switching effect for the oxide systems which have the properties of creating anion deficiency, such as fluorite oxides, rutile and perovskite oxides.

#### Acknowledgments

We thank the financial support from the NSF (Nos. 60621091, 50725209, and 10874218), MOST (Nos. 2006AA03Z402, 2007AA03Z353, and 2007CB936203), and CAS of China.

#### References

- Baikalov, A., Wang, Y.Q., Shen, B., Lorenz, B., Tsui, S., Sun, Y.Y., Xue, Y.Y., Chu, C.W., 2003. Field-driven hysteretic and reversible resistive switch at the  $\text{Ag-Pr}_{0.7}\text{Ca}_{0.3}\text{MnO}_3$  interface. *Applied Physics Letters* 83, 957.
- Beck, A., Bednorz, J.G., Gerber, C., Rossel, C., Widmer, D., 2000. Reproducible switching effect in thin oxide films for memory applications. *Applied Physics Letters* 77, 139.
- Bevan, D.J.M., Kordis, J., 1964. Mixed oxides of the type  $\text{MO}_2$  (fluorite)- $\text{M}_2\text{O}_3$ . 1. Oxygen dissociation pressures and phase relationships in the system  $\text{CeO}_2\text{-Ce}_2\text{O}_3$  at high temperatures. *Journal of Inorganic & Nuclear Chemistry* 26, 1509–1523.
- Crozier, P.A., Wang, R.G., Sharma, R., 2008. In situ environmental TEM studies of dynamic changes in cerium-based oxides nanoparticles during redox processes. *Ultramicroscopy* 108, 1432–1440.
- Fors, R., Khartsev, S.I., Grishin, A.M., 2005. Giant resistance switching in metal-insulator-manganite junctions: evidence for Mott transition. *Physical Review B* 71, 045305–045314.
- Fujii, T., Kawasaki, M., Sawa, A., Akoh, H., Kawazoe, Y., Tokura, Y., 2005. Hysteretic current-voltage characteristics and resistance switching at an epitaxial oxide Schottky junction  $\text{SrRuO}_3/\text{SrTi}_{0.99}\text{Nb}_{0.01}\text{O}_3$ . *Applied Physics Letters* 86, 012107.
- Garvie, L.A.J., Buseck, P.R., 1999. Determination of  $\text{Ce}^{4+}/\text{Ce}^{3+}$  in electron-beam-damaged  $\text{CeO}_2$  by electron energy-loss spectroscopy. *Journal of Physics and Chemistry of Solids* 60, 1943–1947.
- Hamaguchi, M., Aoyama, K., Asanuma, S., Uesu, Y., Katsufuji, T., 2006. Electric-field-induced resistance switching universally observed in transition-metal-oxide thin films. *Applied Physics Letters* 88, 142508.
- Janousch, M., Meijer, G.I., Staub, U., Delley, B., Karg, S.F., Andreasson, B.P., 2007. Role of oxygen vacancies in Cr-doped  $\text{SrTiO}_3$  for resistance-change memory. *Advanced Materials* 19, 2232–+.
- Jooss, C., Wu, L., Beetz, T., Klie, R.F., Beleggia, M., Schofield, M.A., Schramm, S., Hoffmann, J., Zhu, Y., 2007. Polaron melting and ordering as key mechanisms for colossal resistance effects in manganites. *Proceedings of the National Academy of Sciences of the United States of America* 104, 13597–13602.
- Koelling, D.D., Boring, A.M., Wood, J.H., 1983. The electronic-structure of  $\text{CeO}_2$  and  $\text{PrO}_2$ . *Solid State Commun.* 47, 227–232.
- Liu, S.Q., Wu, N.J., Ignatiev, A., 2000. Electric-pulse-induced reversible resistance change effect in magnetoresistive films. *Applied Physics Letters* 76, 2749.
- Nian, Y.B., Strozier, J., Wu, N.J., Chen, X., Ignatiev, A., 2007. Evidence for an oxygen diffusion model for the electric pulse induced resistance change effect in transition-metal oxides. *Physical Review Letters* 98, 146403.
- Oka, T., Nagaosa, N., 2005. Interfaces of correlated electron systems: proposed mechanism for colossal electroresistance. *Physical Review Letters* 95, 266403.
- Prokofiev, A.V., Shelykh, A.I., Melekh, B.T., 1996. Periodicity in the band gap variation of  $\text{Ln}(\text{2X})\text{3}$  ( $\text{X} = \text{O}, \text{S}, \text{Se}$ ) in the lanthanide series. *Journal of Alloys and Compounds* 242, 41–44.
- Quintero, M., Levy, P., Leyva, A.G., Rozenberg, M.J., 2007. Mechanism of electric-pulse-induced resistance switching in manganites. *Physical Review Letters* 98, 116601.
- Rozenberg, M.J., Inoue, I.H., Sanchez, M.J., 2004. Nonvolatile memory with multi-level switching: a basic model. *Physical Review Letters* 92, 178302.
- Sawa, A., Fujii, T., Kawasaki, M., Tokura, Y., 2004. Hysteretic current-voltage characteristics and resistance switching at a rectifying  $\text{Ti}/\text{Pr}_{0.7}\text{Ca}_{0.3}\text{MnO}_3$  interface. *Applied Physics Letters* 85, 4073.

- Shang, D.S., Chen, L.D., Wang, Q., Wu, Z.H., Zhang, W.Q., Li, X.M., 2007. Asymmetric fatigue and its endurance improvement in resistance switching of Ag–La<sub>0.7</sub>Ca<sub>0.3</sub>MnO<sub>3</sub>–Pt heterostructures. *Journal of Physics D: Applied Physics* 40, 5373–5376.
- Sharma, R., Crozier, P.A., Kang, Z.C., Eyring, L., 2004. Observation of dynamic nanostructural and nanochemical changes in ceria-based catalysts during in-situ reduction. *Philosophical Magazine* 84, 2731–2747.
- Skorodumova, N.V., Simak, S.I., Lundqvist, B.I., Abrikosov, I.A., Johansson, B., 2002. Quantum origin of the oxygen storage capability of ceria. *Physical Review Letters* 89, 166601.
- Szot, K., Speier, W., Bihlmayer, G., Waser, R., 2006. Switching the electrical resistance of individual dislocations in single-crystalline SrTiO<sub>3</sub>. *Nature Materials* 5, 312–320.
- Trovarelli, A., 1996. Catalytic properties of ceria and CeO<sub>2</sub>-containing materials. *Catalysis Reviews: Science and Engineering* 38, 439–520.
- Tsui, S., Wang, Y.Q., Xue, Y.Y., Chu, C.W., 2006. Mechanism and scalability in resistive switching of metal–Pr<sub>0.7</sub>Ca<sub>0.3</sub>MnO<sub>3</sub> interface. *Applied Physics Letters* 89, 123502.
- Wang, Z.L., Kang, Z.C., 1998. *Functional and Smart Materials: Structural Evolution and Structure Analysis*. Plenum Press, New York/London.
- Waser, R., Aono, M., 2007. Nanoionics-based resistive switching memories. *Nature Materials* 6, 833–840.
- Yang, J.J., Pickett, M.D., Li, X.M., Ohlberg, D.A.A., Stewart, D.R., Williams, R.S., 2008. Memristive switching mechanism for metal/oxide/metal nanodevices. *Nature Nanotechnology* 3, 429–433.
- Yang, J.J., Miao, F., Pickett, M.D., Ohlberg, D.A.A., Stewart, D.R., Lau, C.N., Williams, R.S., 2009. The mechanism of electroforming of metal oxide memristive switches. *Nanotechnology* 20, 215201–215209.
- Yoshida, C., Kinoshita, K., Yamasaki, T., Sugiyama, Y., 2008. Direct observation of oxygen movement during resistance switching in NiO/Pt film. *Applied Physics Letters* 93, 043106.